

TraceNAS: Zero-shot LLM Pruning via Gradient Trace Correlation

Prajna G. Malettira¹ Manish Nagaraj¹ Arjun Roy¹ Shubham Negi^{1,2,‡} Kaushik Roy¹

Abstract

Structured pruning is essential for efficient deployment of Large Language Models (LLMs). The varying sensitivity of LLM sub-blocks to pruning necessitates the identification of optimal non-uniformly pruned models. Existing methods evaluate the importance of layers, attention heads, or weight channels in isolation. Such localized focus ignores the complex global structural dependencies that exist across the model. Training-aware structured pruning addresses global dependencies, but its computational cost can be just as expensive as post-pruning training. To alleviate the computational burden of training-aware pruning and capture global structural dependencies, we propose TraceNAS, a training-free Neural Architecture Search (NAS) framework that jointly explores structured pruning of LLM depth and width. TraceNAS identifies pruned models that maintain a high degree of loss landscape alignment with the pretrained model using a scale-invariant zero-shot proxy, effectively selecting models that exhibit maximal performance potential during post-pruning training. TraceNAS is highly efficient, enabling high-fidelity discovery of pruned models on a single GPU in 8.5 hours, yielding a 10 \times reduction in GPU-hours compared to training-aware methods. Evaluations on the Llama and Qwen families demonstrate that TraceNAS is competitive with training-aware baselines across commonsense and reasoning benchmarks.

1 Introduction

Recent breakthroughs in Large Language Models (LLMs) (Anthropic, 2023; OpenAI, 2023) have delivered unprecedented capabilities but require massive scale in parameters and computation. Foundational scaling laws (Kaplan et al., 2020) have established that smaller

¹Purdue University ²Google [‡]Work done while at Purdue University. Correspondence to: Prajna G. Malettira <pmaletti@purdue.edu>.

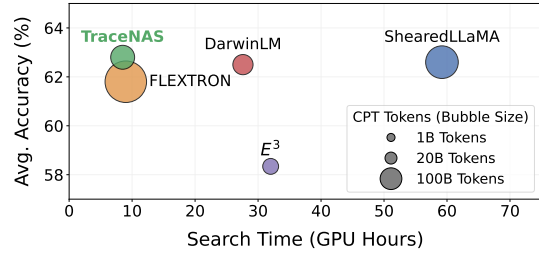


Figure 1. Search Efficiency. TraceNAS identifies optimal non-uniform architectures in 8.5 GPU hours³, achieving competitive accuracy with 10 \times less search overhead than training-aware baselines. The area of the bubble is proportional to the total tokens used for recovery training, highlighting that TraceNAS identified architectures have high recovery potential.

LMs are less sample-efficient, and thus training them from scratch is a resource-intensive bottleneck. Model compression enables the realization of efficient models that preserve the extensive knowledge of the pretrained base. Techniques such as quantization (Frantar et al., 2022; Liu et al., 2024), distillation (Sarah et al., 2024; Li & Jin, 2022) and pruning (Xia et al., 2023; Sun et al., 2023) have become essential, allowing for the accessible deployment of high-performance architectures. Among these, structured pruning (Ma et al., 2023) aims to remove architectural units like attention heads, weight columns, or transformer blocks to achieve immediate hardware speedup. This process can be naturally formulated as a Neural Architecture Search (NAS) (Sieberling et al.; Tao et al., 2023; Tang et al., 2025) problem, where the pretrained LLM is conceptualized as a super-network (Yu et al., 2020; Cai et al., 2019) that serves as the search space.

Structured pruning is inherently more disruptive than the localized masking used in unstructured pruning (Sun et al., 2023; An et al., 2024; Frantar & Alistarh, 2023). While unstructured methods leave the model’s architecture intact, structured pruning physically alters it and risks severing critical pathways in the representational flow. The primary bottleneck in adapting unstructured methods to structured pruning is the lack of a comparable global metric across the model’s layers (Ma et al., 2023). Local importance heuristics such as activation-weighted magnitudes (Sun et al., 2023; An et al., 2024) or Hessian-based reconstruc-

³TraceNAS, ShearedLLaMA and Flextron report search time on a NVIDIA A100, DarwinLM on L40S and E³ reports NPU hours.

tions (Frantar & Alistarh, 2023) identify redundancy within isolated layers and are often incomparable across model depth due to varying magnitude scales (Ma et al., 2023). We address this limitation by utilizing gradients (Das et al., 2023; Yang et al., 2025) as global signals that naturally capture the complex inter-dependencies across the model.

Previous search methods for structured pruning employ mask learning (Xia et al., 2023; Yuan et al., 2025a) or training-aware search (Tang et al., 2025; Bercovich et al., 2025). While these training-aware approaches define the state-of-the-art, they demand substantial computational resources. This overhead stems from the iterative gradient updates required for *training-aware* model discovery and also necessitates a continuous stream of unseen tokens to prevent pruned models from overfitting to calibration data. This cost can make the search for an efficient model just as demanding as post-pruning recovery, motivating the need for *training-free* NAS (Wu et al., 2021; Tran et al., 2021; Ingolfsson et al., 2022) using zero-shot performance proxies. However, existing proxies are primarily designed to identify trainable, randomly initialized architectures by focusing on heuristics such as gradient stability (Abdelfattah et al., 2021) or loss landscape smoothness (Li et al., 2023). These metrics are insufficient for LLM pruning as they prioritize trainability, the ability of a network to learn from scratch. In contrast, the performance of pruned LLMs depends on inheritance, the ability of the pruned model to recover performance by preserving the pretrained loss landscape (Frankle & Carbin, 2018; Frankle et al., 2020; Chen et al., 2020).

In this paper, we introduce TraceNAS, a training-free NAS framework for joint depth and width pruning of LLMs. Our approach leverages the observation that a pretrained model resides in broad, stable regions of the loss landscape (Frankle et al., 2020; Li et al., 2018). We propose a zero-shot proxy that utilizes gradient trace to capture the impact of structural pruning on model sensitivity. Specifically, the proxy measures the sparsity-weighted aggregate over the Pearson Correlation coefficients between the gradient traces of the pruned and pretrained base models. Since structured pruning alters activation and gradient magnitudes, the use of Pearson Correlation ensures scale invariance, thus capturing the alignment of gradient traces on the pretrained loss landscape independently of scale shifts.

To ensure the search remains tractable across varying model scales, we compute these gradients within a low-rank (Hu et al., 2022; Zhao et al., 2024) subspace. By leveraging the intrinsic low-dimensionality (Aghajanyan et al., 2021) of LLMs, TraceNAS captures the principal gradient components of the model while reducing memory overhead by orders of magnitude. Unlike training-aware methods which require significant memory overhead to maintain optimizer states and activations for backpropagation across a large

set of calibration tokens, our training-free approach only requires the gradients of each candidate computed on a minimal calibration set. This reduction in memory consumption enables high-fidelity model discovery (Fig. 1), bypassing the compute intensive requirements typical of training-aware NAS. The primary contributions of this work are:

1. **Scalable Training-free NAS Framework:** We introduce TraceNAS, a unified pruning framework (Fig. 2) for the joint optimization of LLM depth and width. Our approach enables the zero-shot discovery of non-uniform pruned models, facilitating efficient compression across model scales without search-time training.
2. **Zero-shot Proxy for Functional Inheritance:** We introduce a scale-invariant, gradient-based zero-shot proxy that evaluates gradient alignment between the pruned and pretrained models. Our proxy achieves superior Spearman Rho (Spearman, 1961) ($\rho = 0.94$) and Kendall Tau (Kendall, 1938) ($\tau = 0.82$) correlations with downstream accuracy, enabling accurate zero-shot discovery.
3. **Efficient Architecture Discovery:** We show that TraceNAS achieves a $10\times$ reduction in both GPU-hours and total calibration data compared to training-aware methods (Fig. 1). This drastically lowers the overhead for large-scale model compression by ensuring search costs are significantly lower than recovery training.

2 Related Work

2.1 Language Model (LM) Pruning

LLM pruning methods vary by granularity: unstructured weight sparsification (Frantar & Alistarh, 2023) or structured removal (Ma et al., 2023; Kim et al., 2024) of transformer blocks, attention heads or weight channels. These methods are further categorized by their computational complexity relative to the model’s hidden dimension d . Early $O(d)$ magnitude pruning (Han et al., 2015) methods evaluate weights in isolation, ignoring the outlier features characteristic of LLMs (Kovaleva et al., 2021; Luo et al., 2021; Yin et al., 2023). To preserve these outliers, $O(d^2)$ metrics like Wanda (Sun et al., 2023) and FLAP (An et al., 2024) utilize weight-activation products. Furthermore, $O(d^3)$ optimization-based methods like SparseGPT (Frantar & Alistarh, 2023) and LLM-Pruner (Ma et al., 2023) utilize second-order inverse Hessians (Hassibi et al., 1993) to minimize layer-wise reconstruction error. However, these local heuristics prioritize layer properties and fail to account for how pruning-induced errors propagate through the model.

2.2 Influence-based Importance

Beyond these heuristics, recent research has explored influence functions (IF) (Koh & Liang, 2017; Kwon et al., 2023) to better capture how model perturbations affect sen-

sitivity. For instance, LayerIF (Askari et al., 2025) uses IF to estimate layer importance; however, it remains locally heuristic as it perturbs layers individually to measure validation loss sensitivity. This inherently fails to capture the joint impact of multi-layer and width pruning on the model’s representation. Furthermore, the $O(d^3)$ complexity of standard IF is prohibitive for LLMs, requiring inverse Hessian computations for all model parameters. In contrast, TraceNAS adopts an efficient first-order gradient-tracing approach inspired by TracIn (Pruthi et al., 2020) to evaluate the global impact of pruning. By operating with $O(d^2)$ complexity, TraceNAS identifies non-uniform pruned architectures that maintain functional alignment with the pretrained base model, bypassing the computational bottlenecks and local limitations of LayerIF. We provide a detailed comparison between IF, IF-based pruning and TraceNAS in B.1.

2.3 Training-Aware LM Pruning

Recent structured pruning methods, such as ShearedLlama (Xia et al., 2023) and E³ (Yuan et al., 2025b), use mask learning via L_0 regularization and differential mask optimization. While effective, these methods target uniform sparsity across layers, failing to account for the heterogeneous importance distribution across a model’s width (Tao et al., 2023). This has prompted a shift toward discovering non-uniform architectures via evolution search. Methods like SIMPLE (Tao et al., 2023) and EvoPress (Sieberling et al.) employ evolutionary optimization for heterogeneous discovery. On the other hand, DarwinLM (Tang et al., 2025) uses a curriculum-style training-aware search, performing lightweight fine-tuning for every searched candidate. Similarly, PUZZLE (Bercovich et al., 2025) utilizes distillation-based NAS to identify optimal configurations by minimizing block-wise KL divergence. However, the training-aware search inherent to these methods mean their model discovery can be just as computationally intensive as the post-pruning recovery training.

2.4 Zero-shot NAS for LM Pruning

As models scale, these training-intensive searches become intractable, necessitating training-free solutions for NAS. Existing proxies are formulated to identify trainable, randomly initialized architectures by focusing on heuristics such as gradient stability (Abdelfattah et al., 2021), model expressivity (Mellor et al., 2021; Jiang et al., 2023), or loss landscape smoothness (Li et al., 2023). These proxies are insufficient for evaluating pruned models as they do not account for how well a model inherits pretrained knowledge. To address this, recent works LPZero (Dong et al., 2024a) and Pruner-Zero (Dong et al., 2024b) formulate zero-shot pruned model discovery as a two-fold problem: first searching for unique symbolic pruning metrics for the target pretrained model, and subsequently applying these metrics to discover the optimal structured (Dong et al., 2024a) or un-

structured (Dong et al., 2024b) sub-network. While modular, the dual-stage process adds overhead to the search pipeline. In contrast, TraceNAS introduces a unified training-free fitness proxy that directly evaluates a compressed model’s functional alignment with its pretrained base, streamlining the search for pruned models that have high performance potential and fast convergence during post-pruning recovery.

3 Methodology

3.1 Problem Definition

We formulate pruned model discovery as a constrained discrete search over a pretrained super-network, \mathcal{M}_{base} (Cai et al., 2019; Yu et al., 2020). We seek an optimal $\mathcal{M}_{sub} \in \mathcal{G}$ that maximizes a training-free proxy $\Phi(\cdot, \cdot)$, that measures functional inheritance; the ability of \mathcal{M}_{sub} to recover performance by preserving the gradient direction of \mathcal{M}_{base} on its loss landscape:

$$\hat{\mathcal{M}}_{sub} = \arg \max_{\mathcal{M} \in \mathcal{G}} \Phi(\mathcal{M}_{sub}, \mathcal{M}_{base}) \text{ s.t. } \mathcal{P}(\mathcal{M}_{sub}) \leq C,$$

where \mathcal{G} is the search space, $\mathcal{P}(\cdot)$ denotes the parameter count, and C is the target constraint. By maximizing Φ , we identify models with maximal potential for performance recovery during post-pruning *continued pretraining* (CPT) without the overhead of search-time training.

3.2 Search Space Encoding

The search space \mathcal{G} is defined as a joint distribution over the model’s depth and sub-block-wise width, enabling the discovery of non-uniformly pruned architectures from \mathcal{M}_{base} . By operating at sub-block granularity, the TraceNAS search framework treats attention and MLP modules as independent units, thereby capturing diverse structural sparsity.

Architecture Encoding A candidate \mathcal{M}_{sub} is parameterized by a tuple $(\mathbf{d}, \boldsymbol{\kappa})$. The depth configuration $\mathbf{d} \in \{0, 1\}^L$ is a discrete mask over the L blocks of \mathcal{M}_{base} . Setting $d_l = 0$ deactivates the l -th block while preserving the residual stream, allowing the search to explore varying model depths. We enforce a minimum depth constraint, $\sum d_l \geq L_{min}$, to ensure sufficient computational capacity for sequential reasoning. Simultaneously, the width configuration $\boldsymbol{\kappa} = \{\kappa_1, \dots, \kappa_L\}$ where $\kappa_l = (r_{attn}^{(l)}, r_{mlp}^{(l)}) \in (0, 1]$ defines the parameter retention ratio for each attention and MLP sub-block. By decoupling the sparsity ratios, our framework identifies heterogeneous architectures that distinctly prioritize retention in sensitive sub-modules while respecting the global budget C .

3.3 In-Place Architectural Realization

We realize candidate sub-networks \mathcal{M}_{sub} by mapping sparsity ratios $\boldsymbol{\kappa}$ to binary masks and implementing them via an efficient in-place masking strategy.

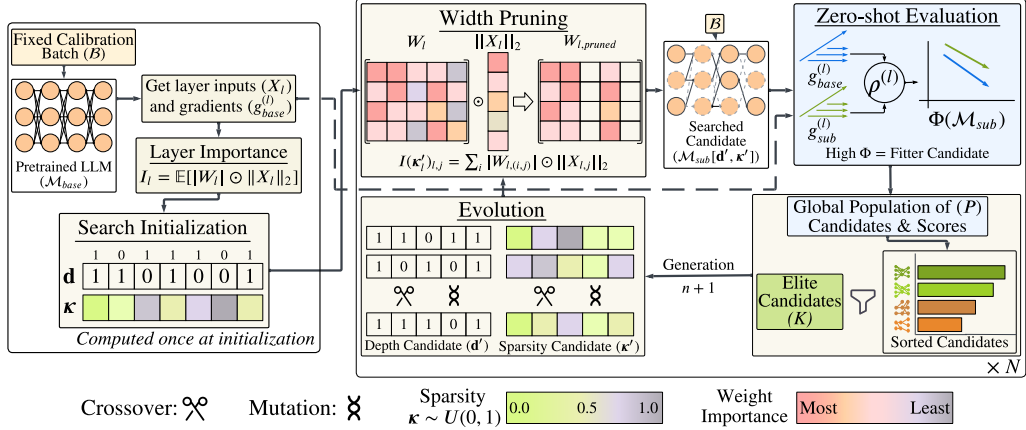


Figure 2. Visualization of the TraceNAS search framework. TraceNAS uses a gradient-based, training-free proxy to guide structural pruning. Following a one-time initialization of base gradient traces (g_{base}) and importance scores (I_l), a population of depth (d) and width (κ) candidates undergoes iterative evolution via crossover and mutation. Each width configuration is realized using an $O(d^2)$ activation-weighted heuristic. Subsequently, candidates \mathcal{M}_{sub} are ranked by the zero-shot proxy Φ , which measures the gradient trace alignment between the active layers of \mathcal{M}_{sub} relative to \mathcal{M}_{base} .

Width Mask Generation To realize a layer’s width configuration κ_l into a weight mask, we use the activation-weighted product: $I(\kappa_l)_{l,j} = \sum_i |W_{l,(ij)}| \odot \|X_{l,j}\|_2$ (Sun et al., 2023) as a saliency metric. This approach explicitly accounts for the outlier features characteristic of LLMs (Kovaleva et al., 2021; Luo et al., 2021; Yin et al., 2023) by scaling weight magnitudes by the L_2 -norm of their corresponding input activations. By identifying channels that are functionally critical to the model’s representational flow, $I(\kappa_l)_{l,j}$ ensures that mask realizations are tailored to preserve the underlying representation of \mathcal{M}_{base} .

Adopting this $O(d^2)$ heuristic avoids the $O(d^3)$ bottleneck of second-order reconstruction methods (Frantar & Alistarh, 2023; Ma et al., 2023; Tang et al., 2025), enabling the high-frequency scoring and realization of hundreds of distinct candidates during the evolutionary search. Crucially, while $I(\kappa_l)_{l,j}$ provides a local channel-selection heuristic, the global distribution of the sparsity ratios κ_l is governed by the TraceNAS proxy Φ (Sec. 3.4), which accounts for the inter-layer dependencies and impact of pruning that local heuristics ignore.

In-Place Masking To score pruned candidates, we use an in-place masking strategy that operates directly on the weight matrices of \mathcal{M}_{base} . This eliminates the need for instantiating the population of candidate models during each search iteration. For depth exploration, \mathcal{M}_{base} is modified according to $d_l \in \mathbf{d}$; if $d_l = 0$, the entire block is bypassed and activations are routed through the residual connection, ensuring functional continuity (Veit et al., 2016; Gromov et al., 2024). For active blocks ($d_l = 1$) the binary masks are applied via a temporary modify-then-restore pointer: $W'_{base} = W_{base} \odot \text{Mask}(\kappa_l)$. This allows the search framework to execute forward and backward passes over a calibration set to capture the cumulative effects of pruning without

the memory overhead of instantiating \mathcal{M}_{sub} . Once the gradient trace is recorded for scoring, the original weights are restored, preserving \mathcal{M}_{base} for subsequent search iterations.

3.4 TraceNAS: Evaluating Functional Alignment

To evaluate the functional integrity of realized candidates \mathcal{M}_{sub} , we propose the proxy Φ . Structured pruning induces a significant representational shift that manifests as an immediate drop in performance (Tran et al., 2022). This initial shock obscures the distinction between fundamental structural collapse and architectures that preserve the essential representational pathways required for effective post-pruning recovery.

Furthermore, as discussed in Sec. 2.1, importance-based metrics (Sun et al., 2023; An et al., 2024) prioritize local weight properties while overlooking the structural interdependencies captured by gradients (Das et al., 2023). To address this, we define Φ as a zero-shot, gradient-based proxy that quantifies functional inheritance. Φ measures the directional alignment between the gradient trace of \mathcal{M}_{sub} and \mathcal{M}_{base} . This directional alignment allows Φ to identify models that are favorably positioned within the pretrained convergence basin, thereby enhancing their potential for functional recovery.

Establishing the Functional Anchor We define the optimal functional state as the gradient trace g_{base} of the pretrained model \mathcal{M}_{base} . Using a calibration set \mathcal{B} , g_{base} provides the directional anchor within the optimization landscape that sub-networks \mathcal{M}_{sub} must align with to ensure functional inheritance. The gradient traces for the base and candidate models are calculated as

$$g = \mathbb{E}_{b \in \mathcal{B}} [\nabla_{\theta} \mathcal{L}(\mathcal{M}(b; \theta))]$$

where θ denotes the trainable model parameters.

Low-Rank Gradient Manifold To ensure computationally tractability across model sizes, we compute gradient traces g within a low-rank subspace. Since storing full-rank LLM gradients is memory-prohibitive, we attach Low-Rank Adapters (LoRA) (Hu et al., 2022) to all linear projections. This approach leverages the observation that the functional knowledge of LLMs resides within a low-dimensional manifold (Aghajanyan et al., 2021; Zhao et al., 2024), allowing us to capture global dependencies while significantly reducing the memory footprint of gradient storage.

Measuring Functional Alignment To quantify how effectively \mathcal{M}_{sub} inherits the functional state of \mathcal{M}_{base} , we calculate the Pearson Correlation Coefficient $\rho^{(l)}$ per layer $l \in L$. For each transformer-block l , $\rho^{(l)}$ measures the alignment between the low-rank gradient traces of the pruned attention and MLP sub-blocks:

$$\rho^{(l)} = \frac{1}{N_l} \left\langle \left(\frac{g_{sub}^{(l)} - \mu_{g_{sub}^{(l)}}}{\sigma_{g_{sub}^{(l)}}} \right), \left(\frac{g_{base}^{(l)} - \mu_{g_{base}^{(l)}}}{\sigma_{g_{base}^{(l)}}} \right) \right\rangle \quad (1)$$

where N_l is the dimensionality of the low-rank subspace, and μ , σ denote the mean and standard deviation of the gradient elements. By standardizing the traces, we decouple the directional alignment from magnitude shifts inherently induced by structural pruning.

Sparsity-Weighted Aggregation We formulate the final proxy Φ by aggregating sub-block correlations using a sparsity-weighted summation. While gradient standardization ensures local scale-invariance, a uniform average of $\rho^{(l)}$ across layers fails to account for the heterogeneous representation capacity of \mathcal{M}_{sub} . We therefore weight each correlation coefficient by its corresponding retention ratio $r^{(l)} \in \kappa_l$:

$$\Phi(\mathcal{M}_{sub}, \mathcal{M}_{base}) = \sum_{l \in \text{Attn}} r_{attn}^{(l)} \cdot \rho^{(l)} + \sum_{l \in \text{MLP}} r_{mlp}^{(l)} \cdot \rho^{(l)} \quad (2)$$

This formulation anchors the global score in the high-capacity regions of \mathcal{M}_{sub} , prioritizing the sub-blocks that serve as the primary repositories of functional inheritance. By weighting $\rho^{(l)}$ by parameter density, we prevent Φ from being skewed by the high-variance noise typical of aggressively pruned sub-blocks.

3.5 Selection & Evolutionary Mechanics

To navigate the discrete search space \mathcal{G} , we employ an evolutionary strategy driven by the proxy Φ . The initial search population P_0 is generated using a global importance prior; detailed initialization procedures and a search convergence analysis are provided in Appendix A.

Search Space Evolution We employ a hybrid evolution strategy for the joint (\mathbf{d}, κ) search space. Depth evolution explores discrete block configurations via contiguous-range crossover and bit-flip mutations. Simultaneously, width evolution explores continuous sparsity ratios using interpolation

crossover and multiplicative Gaussian jitter-based mutation. This joint evolution allows TraceNAS to explore the architectural trade-offs between depth and width while adhering to the constraint C .

Search Granularity The activations used for mask generation are obtained at the attention output (W_o) and MLP down (W_{down}) projection layers. These projections consolidate sub-block representations, and their input activations serve as proxies for the importance of preceding upstream weights. Once generated, these masks are applied to the corresponding projections: W_q, W_k, W_v for attention and W_{up}, W_{gate} for MLP. For Grouped-Query Attention (GQA) (Ainslie et al., 2023) models, we do not prune W_k and W_v to ensure KV-cache compatibility. Furthermore, pruned MLP hidden dimensions are rounded to multiples of $m = 32$ to maintain efficient tensor operations.

3.6 Interpreting Functional Inheritance through Gradient Trace Alignment

The effectiveness of Φ as a proxy for functional inheritance is driven by three key observations:

- **Manifold Anchoring:** High-performing pretrained models reside within flat, stable convergence basins (Frankle et al., 2020; Li et al., 2018). A high alignment score Φ implies that the first-order Taylor expansion of the sub-network’s loss surface remains congruent with that of the base model. By preserving the gradient’s directional signature, \mathcal{M}_{sub} remains anchored within the original functional manifold. This ensures that post-pruning recovery initiates from a region of high directional certainty, enabling a stable loss trajectory rather than necessitating a costly search for a new local minimum.
- **Global Sensitivity via Chain-Rule:** Unlike metrics that evaluate layers in isolation (Sun et al., 2023; Askari et al., 2025), g_{sub} is computed via backpropagation through the masked computational graph. This captures inter-layer disruptions: if an upstream block bottlenecks the representational flow, subsequent layer gradient traces will de-correlate from the base model optimization manifold. This causes a sharp drop in Φ , allowing the proxy to detect structural incoherence and broken residual streams that local heuristics are inherently blind to.
- **Intrinsic Dimensionality Invariance:** Empirical evidence shows that gradient alignment is largely rank-invariant (Fig. 3c, Appendix C.3). This indicates that Φ can capture a pruned model’s functional capability within a low-dimensional (Aghajanyan et al., 2021) manifold. This robustness ensures that the relative performance ranking of candidates remains stable across gradient ranks (Zhao et al., 2024), justifying the use of low-rank subspaces as a reliable and scalable surrogate

for full-rank analysis.

4 Experiments

4.1 Experimental Setup

Models and Datasets: We evaluate TraceNAS across multiple scales using Llama-2-7B (Touvron et al., 2023), Llama-3.1-8B (Dubey et al., 2024) and Qwen-2.5-14B, covering both Multi-Head Attention (MHA) (Vaswani et al., 2017) and Grouped-Query Attention (GQA) (Ainslie et al., 2023) architectures. We use the FineWeb-Edu (Penedo et al., 2024) 100BT dataset for both evolutionary search and post-pruning CPT. For the search, we use a fixed calibration set of 65,536 tokens (16 sequences) per pruned candidate to evaluate a total population of 1500 candidates. This is followed by 20B tokens of post-pruning CPT. Results on additional models and CPT token budgets is provided in Appendix D.2 and D.3.

Implementation Details The evolutionary search is performed with a population of 30 candidates over 50 search iterations. On a single NVIDIA H200 GPU, the search concludes in ~ 2 hours, a significant acceleration over the 8.5-hour A100 baseline reported in Fig. 1. The highest scored sub-networks then undergo CPT on a cluster of six H200 GPUs (~ 16 hours) using a global batch size of 1024 and peak learning rate of $1e^{-4}$. We use a Warmup-Stable-Decay (WSD) (Hu et al., 2024) scheduler, with context lengths set to 4096 for Llama-2 and Qwen-2.5, and 8192 for Llama-3.1. Detailed hyperparameters are available in Appendix A.3.

Baselines: We benchmark TraceNAS against leading structured and layer-pruning methods. This includes, mask-learning methods, ShearedLLaMA (Xia et al., 2023) and E^3 -Pruner (Yuan et al., 2025a), which employ Lagrangian optimization. For training-aware pruning, we compare against DarwinLM (Tang et al., 2025). We further evaluate against Minitron (Sreenivas et al., 2024), Flextron (Cai et al., 2024), LoRAP (Li et al., 2024) and uniformly pruned models found via TraceNAS to isolate the benefits of non-uniform pruning. Comparisons with unstructured pruning methods like Wanda (Sun et al., 2023), FLAP (An et al., 2024) and PrunerZero (Dong et al., 2024b) are included in Appendix D.4.

Evaluation Benchmarks: Models are evaluated using the lm-evaluation-harness (Gao et al., 2024) across 0-shot commonsense reasoning benchmarks: ARC-easy (Clark et al., 2018), LogiQA (Liu et al., 2020), PIQA (Bisk et al., 2020), SciQ (Welbl et al., 2017) and BoolQ (Clark et al., 2019). We also report 5-shot performance on MMLU (Hendrycks et al., 2020) and WinoGrande (Sakaguchi et al., 2020), 10-shot on HellaSwag (Zellers et al., 2019), and 25-shot on ARC Challenge (Clark et al., 2018).

4.2 TraceNAS Proxy Validation: Performance Correlation and Stability

To evaluate TraceNAS as a proxy for recovery potential and verify its consistency across hyperparameters, we analyze 70 candidate models sampled from the AmoebaLLM (Fu et al., 2024) search space. This evaluates the proxy in an environment unbiased by our specific evolutionary search or large-scale CPT. We compute Spearman Rho (SP) and Kendall Tau (KT) correlations against Wikitext-2 perplexity (PPL), MMLU accuracy and average downstream accuracy after Once-for-All (OFA) (Cai et al., 2019; Sukthanker et al.) finetuning on Alpaca (Taori et al., 2023).

Table 1. Correlation of zero-shot proxies with model performance calculated over 70 pruned models and averaged over 3 seeds. We report Spearman Rho (SP) and Kendall Tau (KT) for perplexity (PPL), MMLU and average commonsense reasoning accuracies. Best correlation values per column are **bolded** and underlined values denote second best correlation.

Method	PPL		MMLU		Avg. Acc.	
	SP	KT	SP	KT	SP	KT
#Params	0.87	0.72	0.11	0.07	0.66	0.50
NASWOT	0.69	0.50	0.35	0.26	0.39	0.29
ZiCo	0.87	0.72	0.11	0.07	0.66	0.50
GradNorm	0.93	0.79	0.45	0.32	<u>0.93</u>	0.78
Synaptic Saliency	0.93	0.78	0.37	0.25	0.89	0.73
MeCo	0.92	0.79	0.03	0.02	0.75	0.58
PrunerZero	0.44	0.31	0.88	0.69	0.68	0.50
TraceNAS – Dot	0.57	0.46	0.35	0.25	0.58	0.47
TraceNAS – Cosine	0.91	0.77	0.48	0.35	0.91	0.79
TraceNAS – Unweighted	0.85	0.71	0.23	0.16	0.77	0.62
TraceNAS (Ours)	0.93	0.79	<u>0.54</u>	<u>0.39</u>	0.94	0.82

Correlation with Downstream Performance TraceNAS achieves superior ranking correlation with downstream performance, as shown in Table 1. Unlike trainability proxies like NASWOT (Mellor et al., 2021) and ZiCo (Li et al., 2023), which rank models based on their expressivity and convergence capability from random initializations, our proxy explicitly accounts for pretrained knowledge inheritance. By measuring the alignment between the pruned and base model gradient traces, TraceNAS captures how structural changes impact the functional sensitivity of the model. This allows the proxy to account for complex reasoning dependencies that feature-based or loss-landscape smoothness-based metrics fail to capture.

While GradNorm (Abdelfattah et al., 2021) and Synaptic Saliency (Tanaka et al., 2020) effectively rank PPL, they prioritize the health of the gradient signal and whether pruning disproportionately impacts individual layers. This provides an incomplete picture of the candidate’s representational integrity. Similarly, while MeCo (Jiang et al., 2023) performs well on PPL, it fails to translate to task-specific accuracy. PrunerZero (Dong et al., 2024b) achieves the highest correlation on MMLU by incorporating gradient information, but

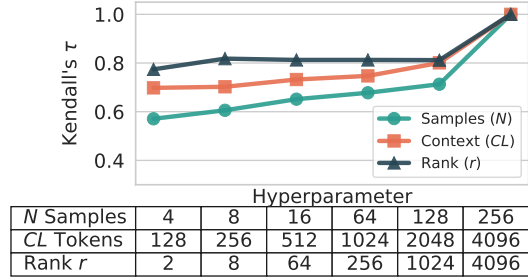


Figure 3. TraceNAS proxy stability analysis. We report Kendall τ correlation between ranking scores across search hyperparameters (a) number of samples (N), (b) context length (CL), and (c) LoRA rank (r) which define the x-axis. High τ values demonstrate that TraceNAS consistently ranks models across search settings.

this success does not generalize to PPL or average downstream accuracy. Additionally, #Params has high ranking potential for both PPL and average accuracy, however this does not translate to a good measure of a model’s knowledge retention capability, which is needed for MMLU. This tells us that while increasing model size is a good indicator of generalizability potential, #Params cannot capture the nuances required to analyze a pruned model’s factual knowledge and reasoning capabilities.

In contrast, TraceNAS maintains superior ranking stability across all three metrics by leveraging Sparsity-Weighted Pearson Correlation (Φ). Φ is specifically designed to isolate functional signals from directional noise through gradient centering. By using layer-wise sparsity as a weighting factor, Φ anchors the global fitness score in high-capacity regions. This prevents the ranking from being skewed by the high variance noise typical of aggressively pruned sub-blocks. We further validate the choice of our proxy by comparing against alternative alignment metrics, including dot product, cosine similarity and unweighted aggregation of Pearson Correlation Coefficients. A detailed analysis of the correlation results is presented in Table 1 is provided in Appendix C.

Hyperparameter Stability Analysis We evaluate the robustness of TraceNAS by computing the Kendall τ correlation between various search hyperparameters and the highest setting in each category ($N = 256$, $CL = 4096$, $r = 4096$). As shown in Fig. 3, the proxy maintains high ranking consistency across all variables, confirming that gradient trace alignment effectively captures model inheritance even under constrained search settings. Our analysis of these internal ranking correlations follows:

- **Number of Calibration Samples (N):** We observe that correlation monotonically align with the $N = 256$ configuration as sample density increases. While ranking sensitivity is present at $N = 4$ with $\tau \approx 0.57$, stability improves significantly to $\tau \approx 0.71$ at $N = 128$. This trend suggests that representative gradient align-

ment is captured with relatively few samples, justifying our sample-efficient search settings.

- **Context Length (CL):** We observe that correlation with $CL = 4096$ remains high across context lengths, rising from $\tau \approx 0.70$ at shorter contexts to $\tau \approx 0.80$ at $CL = 2048$. The high agreement for all $CL \geq 1024$ rankings suggests that the proxy’s saliency is largely preserved once the model captures sufficient long-range dependencies, allowing for significantly reduced compute during pruned model discovery.
- **Low-rank Gradient Subspace (r):** We observe that proxy stability is most significant across varying gradient subspace dimensions. Correlation with the full-rank ($r = 4096$) configuration remains consistently high, exceeding $\tau \approx 0.77$ even at $r = 2$, and peaking at $\tau \approx 0.82$ for $r = 8$ before stabilizing. This validates our use of $r = 64$ during the search, confirming that low-rank gradient traces are sufficient to capture functional nuances while minimizing memory overhead during the search.

Detailed inter-hyperparameter correlations, comparing each configuration directly to downstream task performance, are provided in Appendix C.3.

4.3 Main Results

We evaluate the capability of TraceNAS to discover high performing pruned models by evaluating on Llama-2-7B, Llama-3.1-8B, and Qwen-2.5-14B Instruct to 2.7B, 4.6B, and 8.4B parameters, respectively. As shown in Tables 2 and 3, TraceNAS identifies sub-networks with high sample efficiency, requiring only 98M total search tokens, a 10 \times and 4 \times reduction compared to DarwinLM and ShearedLLaMA, while achieving superior accuracy. This efficiency validates the high ranking capability and stability of our proxy observed in Sec. 4.2.

Performance on Llama-2-7B TraceNAS achieves the highest average accuracy (62.81%) on Llama-2 7B across eight benchmarks, outperforming DarwinLM (62.57%) and ShearedLLaMA (62.63%). To ensure a fair comparison, we retrained DarwinLM and ShearedLLaMA on our 20B token distribution (\dagger). Notably, ShearedLLaMA’s performance drops to 60.86% when restricted to our 20B token budget, highlighting its reliance on high-token-count recovery to reach competitive accuracy. While DarwinLM remains competitive, its performance slightly dips when using our unfiltered FineWeb-Edu samples rather than the highly curated top 0.1 percentile used in its original report.

Furthermore, TraceNAS significantly outperforms LoRAP (Li et al., 2024), E³-Pruner (Yuan et al., 2025a), and our uniform baseline. Our 2.7B model has comparable the performance with Flextron (Cai et al., 2024) despite the latter having a larger parameter footprint and requiring 4.5 \times

TraceNAS: Zero-shot LLM Pruning via Gradient Trace Correlation

Table 2. Pruning results for LLaMA-2-7B. Averages are calculated across eight reasoning benchmarks. TraceNAS achieves highest average accuracy while requiring significantly fewer search tokens.

Method	#Params	Srch	Recv	PIQA	WG	ArcE	ArcC	HS	SciQ	LQA	BQ	Avg.
Llama-2-7B	6.7B	–	–	77.69	74.11	76.34	52.81	78.96	93.80	29.80	77.73	70.16
LoRAP	2.7B	–	–	57.20	47.90	31.30	26.30	30.00	51.20	27.50	61.90	41.66
Flextron	3.4B	1K	90B	74.10	62.00	66.50	–	68.50	–	–	–	–
E ³	2.7B	0.5B	–	71.20	57.30	65.40	38.10	54.60	88.40	28.10	63.60	58.34
ShearedLLaMA	2.7B	0.4B	50B	75.80	64.20	67.00	41.20	70.80	90.80	28.20	63.00	62.63
DarwinLM	2.7B	1.0B	10B	73.12	63.77	69.94	43.94	66.95	90.20	28.57	64.10	62.57
Uniform	3.4B	98M	20B	65.10	58.30	69.50	38.20	54.30	87.10	26.03	59.90	57.30
ShearedLLaMA	2.7B	0.4B	20B [†]	72.92	60.80	67.46	38.06	64.73	90.30	28.72	63.91	60.86
DarwinLM	2.7B	1.0B	20B [†]	73.17	63.59	69.90	42.91	66.57	89.00	29.18	63.63	62.24
TraceNAS (Ours)	2.7B	98M	20B	73.40	63.97	70.20	43.80	68.54	91.10	29.71	61.76	62.81

Table 3. Pruning results for Llama-3.1-8B and Qwen-2.5-14B-Instruct. TraceNAS has the best average accuracy and surpasses baselines on several complex reasoning benchmarks. Averages are calculated across the eight reasoning benchmarks, not including MMLU.

Method	#Params	Srch	Recv	MMLU	PIQA	WG	ArcE	ArcC	HS	SciQ	LQA	BQ	Avg.
Llama-3.1-8B	8B	–	–	64.78	81.22	77.42	81.64	57.59	81.81	96.20	31.02	82.14	73.63
Minitron	4.4B	–	94B	60.50	76.82	73.50	76.89	56.14	76.03	96.20	31.02	83.14	71.22
DarwinLM	4.6B	1B	10B	43.21	74.59	65.03	73.27	51.27	71.13	93.40	30.72	71.00	66.30
Uniform (Ours)	4.6B	98M	20B	28.76	68.32	58.54	68.23	47.89	66.42	88.48	27.54	66.59	61.50
DarwinLM	4.6B	1B	20B [†]	43.32	74.53	65.26	73.13	51.62	71.17	93.24	30.76	70.08	66.22
TraceNAS (Ours)	4.6B	98M	20B	30.12	74.23	66.08	73.50	52.26	69.01	93.90	30.81	73.00	66.60
Qwen-2.5 14B	14B	–	–	82.53	82.10	79.71	85.81	72.44	85.10	96.70	41.16	87.95	78.87
Minitron	8.4B	–	94B	36.10	80.41	80.03	83.38	64.24	83.10	97.10	33.48	84.43	75.77
DarwinLM	8.4B	1B	10B	55.97	78.12	70.63	79.41	57.42	74.93	89.30	33.10	73.57	69.56
E ³	8.2B	0.5B	–	36.50	76.90	63.00	76.00	47.90	67.00	93.70	30.00	66.50	65.13
Uniform (Ours)	8.4B	98M	20B	51.23	71.32	62.64	77.12	50.02	69.89	88.91	28.53	69.45	64.73
DarwinLM	8.4B	1B	20B [†]	56.97	78.17	72.09	79.86	57.03	74.96	90.32	32.80	73.17	69.80
TraceNAS (Ours)	8.4B	98M	20B	58.79	76.63	73.24	81.07	56.05	73.77	95.70	32.56	73.70	70.34

more CPT tokens. The substantial performance gap between TraceNAS and the uniform baseline (5.51% average) underscores the necessity of non-uniform architecture search for maintaining representational integrity. We provide performance scalability results of our Llama-2-2.7B model by evaluating recovery performance at 10B and 50B tokens in Appendix D.3.

Generalization to GQA Architectures Evaluation on Llama-3.1 and Qwen-2.5 demonstrates the generalizability of TraceNAS to GQA architectures. For Llama-3.1-8B, TraceNAS significantly improves upon the uniform baseline (66.60% vs 61.50%) and outperforms DarwinLM across critical reasoning tasks such as ARC-C (52.26%) and BoolQ (73.00%). On Qwen-2.5-14B, TraceNAS maintains its lead with a 70.34% average, surpassing both DarwinLM (69.80%) and E³-Pruner (65.13%).

While Minitron (Sreenivas et al., 2024) achieves higher accuracies across reasoning baseline and TraceNAS models, it requires an intensive 94B tokens for recovery, approximately 4.7 \times the computational cost of TraceNAS. Across all architectures, TraceNAS produces sub-networks whose gradient traces are highly aligned with the pretrained gradients, allowing for high-fidelity recovery and discovered at a fraction of the computational search cost required by existing training-aware methods. Detailed perplexity evaluations across different sparsity levels and a speedup analysis against all publicly available baselines are provided in Appendix C.4 and Appendix D.1, respectively.

ent trace, allowing for high-fidelity recovery and discovered at a fraction of the computational search cost required by existing training-aware methods. Detailed perplexity evaluations across different sparsity levels and a speedup analysis against all publicly available baselines are provided in Appendix C.4 and Appendix D.1, respectively.

5 Conclusion

In this work, we introduce TraceNAS, a zero-shot NAS framework for non-uniform structured pruning of LLMs. By leveraging a novel scale-invariant gradient proxy, TraceNAS identifies sub-networks that maintain high gradient trace alignment with the pretrained base model. This alignment ensures the preservation of functional inheritance, allowing for efficient recovery during continued pretraining. Our framework demonstrates consistent performance gains across Llama-2, Llama-3.1, and Qwen-2.5 architectures, achieving an order-of-magnitude reduction in search overhead compared to training-aware baselines. By eliminating the prohibitive cost of search-time training, TraceNAS provides a scalable and high-fidelity foundation for model compression that effectively retains the complex reasoning capabilities of dense pretrained models.

[†]Models trained on our CPT data setup and the original codebase provided in the respective papers.

Acknowledgments

This work was supported in part by the Center for the Co-Design of Cognitive Systems (COCOSYS), a DARPA-sponsored JUMP center, the Semiconductor Research Corporation (SRC), the National Science Foundation (NSF) and the Department of Energy (DOE).

Impact Statement

The research presented in this paper advances the accessibility of high-performing LLMs by significantly lowering the computational barriers to large-scale model compression. By providing a training-free framework for architectural discovery, we enable the development of efficient models even under resource constraints. Furthermore, the substantial reduction in GPU-hours required for model search directly mitigates the carbon footprint and energy consumption associated with large-scale NAS. These advancements enable the deployment of LLMs in edge environments, supporting sustainable AI development. To promote reproducibility, an anonymous GitHub repository will be made available to reviewers and area chairs during the discussion period, as per the ICML Author Guidelines.

References

Abdelfattah, M. S., Mehrotra, A., Dudziak, Ł., and Lane, N. D. Zero-cost proxies for lightweight nas. *arXiv preprint arXiv:2101.08134*, 2021.

Aghajanyan, A., Gupta, S., and Zettlemoyer, L. Intrinsic dimensionality explains the effectiveness of language model fine-tuning. In Zong, C., Xia, F., Li, W., and Navigli, R. (eds.), *Proceedings of the 59th Annual Meeting of the Association for Computational Linguistics and the 11th International Joint Conference on Natural Language Processing (Volume 1: Long Papers)*, pp. 7319–7328, Online, August 2021. Association for Computational Linguistics. doi: 10.18653/v1/2021.acl-long.568. URL <https://aclanthology.org/2021.acl-long.568/>.

Ainslie, J., Lee-Thorp, J., De Jong, M., Zemlyanskiy, Y., Lebrón, F., and Sanghai, S. Gqa: Training generalized multi-query transformer models from multi-head checkpoints. *arXiv preprint arXiv:2305.13245*, 2023.

An, Y., Zhao, X., Yu, T., Tang, M., and Wang, J. Fluctuation-based adaptive structured pruning for large language models. In *Proceedings of the AAAI Conference on Artificial Intelligence*, volume 38, pp. 10865–10873, 2024.

Anthropic, P. Introducing claudie. *March*, 14:2023, 2023.

Askari, H., Gupta, S., Wang, F., Chhabra, A., and Chen, M. Layerif: Estimating layer quality for large language models using influence functions. *arXiv preprint arXiv:2505.23811*, 2025.

Bercovich, A., Ronen, T., Abramovich, T., Ailon, N., Assaf, N., Dabbah, M., Galil, I., Geifman, A., Geifman, Y., Golan, I., Haber, N., Karpas, E. D., Koren, R., Levy, I., Molchanov, P., Mor, S., Moshe, Z., Nabwani, N., Puny, O., Rubin, R., Schen, I., Shahaf, I., Tropp, O., Argov, O. U., Zilberstein, R., and El-Yaniv, R. Puzzle: Distillation-based NAS for inference-optimized LLMs. In Singh, A., Fazel, M., Hsu, D., Lacoste-Julien, S., Berkenkamp, F., Maharaj, T., Wagstaff, K., and Zhu, J. (eds.), *Proceedings of the 42nd International Conference on Machine Learning*, volume 267 of *Proceedings of Machine Learning Research*, pp. 3806–3830. PMLR, 13–19 Jul 2025. URL <https://proceedings.mlr.press/v267/bercovich25a.html>.

Bisk, Y., Zellers, R., Gao, J., Choi, Y., et al. Piqa: Reasoning about physical commonsense in natural language. In *Proceedings of the AAAI conference on artificial intelligence*, volume 34, pp. 7432–7439, 2020.

Cai, H., Gan, C., Wang, T., Zhang, Z., and Han, S. Once-for-all: Train one network and specialize it for efficient deployment. *arXiv preprint arXiv:1908.09791*, 2019.

Cai, R., Muralidharan, S., Heinrich, G., Yin, H., Wang, Z., Kautz, J., and Molchanov, P. Flextron: Many-in-one flexible large language model. *arXiv preprint arXiv:2406.10260*, 2024.

Chen, T., Frankle, J., Chang, S., Liu, S., Zhang, Y., Wang, Z., and Carbin, M. The lottery ticket hypothesis for pre-trained bert networks. *Advances in neural information processing systems*, 33:15834–15846, 2020.

Clark, C., Lee, K., Chang, M.-W., Kwiatkowski, T., Collins, M., and Toutanova, K. Boolq: Exploring the surprising difficulty of natural yes/no questions. *arXiv preprint arXiv:1905.10044*, 2019.

Clark, P., Cowhey, I., Etzioni, O., Khot, T., Sabharwal, A., Schoenick, C., and Tafjord, O. Think you have solved question answering? try arc, the ai2 reasoning challenge. *arXiv preprint arXiv:1803.05457*, 2018.

Das, R. J., Sun, M., Ma, L., and Shen, Z. Beyond size: How gradients shape pruning decisions in large language models. *arXiv preprint arXiv:2311.04902*, 2023.

Dong, P., Li, L., Liu, X., Tang, Z., Liu, X., Wang, Q., and Chu, X. Lpzero: Language model zero-cost proxy search from zero. *arXiv preprint arXiv:2410.04808*, 2024a.

Dong, P., Li, L., Tang, Z., Liu, X., Pan, X., Wang, Q., and Chu, X. Pruner-zero: Evolving symbolic pruning metric from scratch for large language models. *arXiv preprint arXiv:2406.02924*, 2024b.

Dubey, A., Jauhri, A., Pandey, A., Kadian, A., Al-Dahle, A., Letman, A., Mathur, A., Yang, A., Fan, A., et al. The llama 3 herd of models. *arXiv preprint arXiv:2407.21783*, 2024.

Frankle, J. and Carbin, M. The lottery ticket hypothesis: Finding sparse, trainable neural networks. *arXiv preprint arXiv:1803.03635*, 2018.

Frankle, J., Dziugaite, G. K., Roy, D., and Carbin, M. Linear mode connectivity and the lottery ticket hypothesis. In *International Conference on Machine Learning*, pp. 3259–3269. PMLR, 2020.

Frantar, E. and Alistarh, D. Sparsegpt: Massive language models can be accurately pruned in one-shot. In *International conference on machine learning*, pp. 10323–10337. PMLR, 2023.

Frantar, E., Ashkboos, S., Hoefer, T., and Alistarh, D. Gptq: Accurate post-training quantization for generative pre-trained transformers. *arXiv preprint arXiv:2210.17323*, 2022.

Fu, Y., Yu, Z., Li, J., Qian, J., Zhang, Y., Yuan, X., Shi, D., Yakunin, R., and Lin, Y. C. Amoeballm: Constructing any-shape large language models for efficient and instant deployment. *Advances in Neural Information Processing Systems*, 37:78299–78319, 2024.

Gao, L., Tow, J., Abbasi, B., Biderman, S., Black, S., DiPofi, A., Foster, C., Golding, L., Hsu, J., Le Noac'h, A., Li, H., McDonell, K., Muennighoff, N., Ociepa, C., Phang, J., Reynolds, L., Schoelkopf, H., Skowron, A., Sutawika, L., Tang, E., Thite, A., Wang, B., Wang, K., and Zou, A. The language model evaluation harness, 07 2024. URL <https://zenodo.org/records/12608602>.

Gromov, A., Tirumala, K., Shapourian, H., Glorioso, P., and Roberts, D. A. The unreasonable ineffectiveness of the deeper layers, 2024. URL <https://arxiv.org/abs/2403.17887>, 2024.

Han, S., Mao, H., and Dally, W. J. Deep compression: Compressing deep neural networks with pruning, trained quantization and huffman coding. *arXiv preprint arXiv:1510.00149*, 2015.

Hassibi, B., Stork, D. G., and Wolff, G. J. Optimal brain surgeon and general network pruning. In *IEEE international conference on neural networks*, pp. 293–299. IEEE, 1993.

Hendrycks, D., Burns, C., Basart, S., Zou, A., Mazeika, M., Song, D., and Steinhardt, J. Measuring massive multitask language understanding. *arXiv preprint arXiv:2009.03300*, 2020.

Hu, E. J., Shen, Y., Wallis, P., Allen-Zhu, Z., Li, Y., Wang, S., Wang, L., Chen, W., et al. Lora: Low-rank adaptation of large language models. *ICLR*, 1(2):3, 2022.

Hu, S., Tu, Y., Han, X., He, C., Cui, G., Long, X., Zheng, Z., Fang, Y., Huang, Y., Zhao, W., et al. Minicpm: Unveiling the potential of small language models with scalable training strategies. *arXiv preprint arXiv:2404.06395*, 2024.

Ingolfsson, T. M., Vero, M., Wang, X., Lamberti, L., Benini, L., and Spallanzani, M. Reducing neural architecture search spaces with training-free statistics and computational graph clustering. In *Proceedings of the 19th ACM International Conference on Computing Frontiers*, pp. 213–214, 2022.

Jiang, T., Wang, H., and Bie, R. Meco: zero-shot nas with one data and single forward pass via minimum eigenvalue of correlation. *Advances in Neural Information Processing Systems*, 36:61020–61047, 2023.

Kaplan, J., McCandlish, S., Henighan, T., Brown, T. B., Chess, B., Child, R., Gray, S., Radford, A., Wu, J., and Amodei, D. Scaling laws for neural language models. *arXiv preprint arXiv:2001.08361*, 2020.

Kendall, M. G. A new measure of rank correlation. *Biometrika*, 30(1-2):81–93, 1938.

Kim, B.-K., Kim, G., Kim, T.-H., Castells, T., Choi, S., Shin, J., and Song, H.-K. Shortened llama: A simple depth pruning for large language models. *arXiv preprint arXiv:2402.02834*, 11:1, 2024.

Koh, P. W. and Liang, P. Understanding black-box predictions via influence functions. In *International conference on machine learning*, pp. 1885–1894. PMLR, 2017.

Kovaleva, O., Kulshreshtha, S., Rogers, A., and Rumshisky, A. Bert busters: Outlier dimensions that disrupt transformers. *arXiv preprint arXiv:2105.06990*, 2021.

Kwon, Y., Wu, E., Wu, K., and Zou, J. Datainf: Efficiently estimating data influence in lora-tuned llms and diffusion models. *arXiv preprint arXiv:2310.00902*, 2023.

Li, G., Yang, Y., Bhardwaj, K., and Marculescu, R. Zico: Zero-shot nas via inverse coefficient of variation on gradients. *arXiv preprint arXiv:2301.11300*, 2023.

Li, G., Tang, Y., and Zhang, W. Lorap: Transformer sub-layers deserve differentiated structured compression for large language models. *arXiv preprint arXiv:2404.09695*, 2024.

Li, H., Xu, Z., Taylor, G., Studer, C., and Goldstein, T. Visualizing the loss landscape of neural nets. *Advances in neural information processing systems*, 31, 2018.

Li, L. and Jin, Z. Shadow knowledge distillation: Bridging offline and online knowledge transfer. *Advances in Neural Information Processing Systems*, 35:635–649, 2022.

Liu, J., Cui, L., Liu, H., Huang, D., Wang, Y., and Zhang, Y. Logiqa: A challenge dataset for machine reading comprehension with logical reasoning. *arXiv preprint arXiv:2007.08124*, 2020.

Liu, Z., Oguz, B., Zhao, C., Chang, E., Stock, P., Mehdad, Y., Shi, Y., Krishnamoorthi, R., and Chandra, V. Llm-qat: Data-free quantization aware training for large language models. In *Findings of the Association for Computational Linguistics: ACL 2024*, pp. 467–484, 2024.

Luo, Z., Kulmizev, A., and Mao, X. Positional artefacts propagate through masked language model embeddings. In *Proceedings of the 59th annual meeting of the Association for Computational Linguistics and the 11th international joint conference on natural language processing (volume 1: long papers)*, pp. 5312–5327, 2021.

Ma, X., Fang, G., and Wang, X. Llm-pruner: On the structural pruning of large language models. *Advances in neural information processing systems*, 36:21702–21720, 2023.

Mellor, J., Turner, J., Storkey, A., and Crowley, E. J. Neural architecture search without training. In *International conference on machine learning*, pp. 7588–7598. PMLR, 2021.

Mukherjee, S., Mitra, A., Jawahar, G., Agarwal, S., Palangi, H., and Awadallah, A. Orca: Progressive learning from complex explanation traces of gpt-4. *arXiv preprint arXiv:2306.02707*, 2023.

OpenAI, R. Gpt-4 technical report. arxiv 2303.08774. *View in Article*, 2(5):1, 2023.

Penedo, G., Kydlíček, H., Lozhkov, A., Mitchell, M., Raffel, C. A., Von Werra, L., Wolf, T., et al. The fineweb datasets: Decanting the web for the finest text data at scale. *Advances in Neural Information Processing Systems*, 37: 30811–30849, 2024.

Pruthi, G., Liu, F., Kale, S., and Sundararajan, M. Estimating training data influence by tracing gradient descent. *Advances in Neural Information Processing Systems*, 33: 19920–19930, 2020.

Sakaguchi, K., Le Bras, R., Bhagavatula, C., and Choi, Y. Winogrande: An adversarial winograd schema challenge at scale. In *Proceedings of the AAAI Conference on Artificial Intelligence*, volume 34, pp. 8732–8740, 2020.

Sarah, A., Nittur Sridhar, S., Szankin, M., and Sundaresan, S. Llama-nas: Efficient neural architecture search for large language models. In *European Conference on Computer Vision*, pp. 67–74. Springer, 2024.

Sieberling, O., Kuznedelev, D., Kurtic, E., and Alistarh, D. Evopress: Accurate dynamic model compression via evolutionary search. In *Forty-second International Conference on Machine Learning*.

Spearman, C. The proof and measurement of association between two things. 1961.

Sreenivas, S. T., Muralidharan, S., Joshi, R., Chochowski, M., Mahabaleshwarkar, A. S., Shen, G., Zeng, J., Chen, Z., Suhara, Y., Diao, S., et al. Llm pruning and distillation in practice: The minitron approach. *arXiv preprint arXiv:2408.11796*, 2024.

Sukthanker, R. S., Staffler, B., Hutter, F., and Klein, A. Large language model compression with neural architecture search. In *Workshop on Machine Learning and Compression, NeurIPS 2024*.

Sun, M., Liu, Z., Bair, A., and Kolter, J. Z. A simple and effective pruning approach for large language models. *arXiv preprint arXiv:2306.11695*, 2023.

Tanaka, H., Kunin, D., Yamins, D. L., and Ganguli, S. Pruning neural networks without any data by iteratively conserving synaptic flow. *Advances in neural information processing systems*, 33:6377–6389, 2020.

Tang, S., Sieberling, O., Kurtic, E., Shen, Z., and Alistarh, D. Darwinlm: Evolutionary structured pruning of large language models. *arXiv preprint arXiv:2502.07780*, 2025.

Tao, C., Hou, L., Bai, H., Wei, J., Jiang, X., Liu, Q., Luo, P., and Wong, N. Structured pruning for efficient generative pre-trained language models. In Rogers, A., Boyd-Graber, J., and Okazaki, N. (eds.), *Findings of the Association for Computational Linguistics: ACL 2023*, pp. 10880–10895, Toronto, Canada, July 2023. Association for Computational Linguistics. doi: 10.18653/v1/2023.findings-acl.692. URL <https://aclanthology.org/2023.findings-acl.692/>.

Taori, R., Gulrajani, I., Zhang, T., Dubois, Y., Li, X., Guestrin, C., Liang, P., and Hashimoto, T. B. Stanford alpaca: An instruction-following llama model, 2023.

Touvron, H., Lavril, T., Izacard, G., Martinet, X., Lachaux, M.-A., Lacroix, T., Rozière, B., Goyal, N., Hambro, E., Azhar, F., et al. Llama: Open and efficient foundation language models. *arXiv preprint arXiv:2302.13971*, 2023.

Tran, C., Fioretto, F., Kim, J.-E., and Naidu, R. Pruning has a disparate impact on model accuracy. *Advances in neural information processing systems*, 35:17652–17664, 2022.

Tran, L.-T., Ali, M. S., and Bae, S.-H. A feature fusion based indicator for training-free neural architecture search. *IEEE Access*, 9:133914–133923, 2021.

Vaswani, A., Shazeer, N., Parmar, N., Uszkoreit, J., Jones, L., Gomez, A. N., Kaiser, Ł., and Polosukhin, I. Attention is all you need. *Advances in neural information processing systems*, 30, 2017.

Veit, A., Wilber, M. J., and Belongie, S. Residual networks behave like ensembles of relatively shallow networks. *Advances in neural information processing systems*, 29, 2016.

Wang, Z., Wohlwend, J., and Lei, T. Structured pruning of large language models. In *Proceedings of the 2020 conference on empirical methods in natural language processing (emnlp)*, pp. 6151–6162, 2020.

Welbl, J., Liu, N. F., and Gardner, M. Crowdsourcing multiple choice science questions. *arXiv preprint arXiv:1707.06209*, 2017.

Wu, M.-T., Lin, H.-I., and Tsai, C.-W. A training-free genetic neural architecture search. In *Proceedings of the 2021 ACM International Conference on Intelligent Computing and Its Emerging Applications*, pp. 65–70, 2021.

Xia, M., Gao, T., Zeng, Z., and Chen, D. Sheared llama: Accelerating language model pre-training via structured pruning. *arXiv preprint arXiv:2310.06694*, 2023.

Yang, Y., Zhen, K., Ganesh, B., Galstyan, A., Huybrechts, G., Müller, M., Kübler, J. M., Swaminathan, R. V., Mouchtaris, A., Bodapati, S. B., et al. Wanda++: Pruning large language models via regional gradients. *arXiv preprint arXiv:2503.04992*, 2025.

Yin, L., Wu, Y., Zhang, Z., Hsieh, C.-Y., Wang, Y., Jia, Y., Li, G., Jaiswal, A., Pechenizkiy, M., Liang, Y., et al. Outlier weighed layerwise sparsity (owl): A missing secret sauce for pruning llms to high sparsity. *arXiv preprint arXiv:2310.05175*, 2023.

Yu, J., Jin, P., Liu, H., Bender, G., Kindermans, P.-J., Tan, M., Huang, T., Song, X., Pang, R., and Le, Q. Bignas: Scaling up neural architecture search with big single-stage models. In *European Conference on Computer Vision*, pp. 702–717. Springer, 2020.

Yuan, T., Bai, H., Pan, Y., Cao, X., Zhang, T., Hou, L., Hu, T., and Yu, X. E³-pruner: Towards efficient, economical, and effective layer pruning for large language models. *arXiv preprint arXiv:2511.17205*, 2025a.

Yuan, T., Bai, H., Pan, Y., Cao, X., Zhang, T., Hou, L., Hu, T., and Yu, X. E³-pruner: Towards efficient, economical, and effective layer pruning for large language models, 2025b. URL <https://arxiv.org/abs/2511.17205>.

Zellers, R., Holtzman, A., Bisk, Y., Farhadi, A., and Choi, Y. Hellaswag: Can a machine really finish your sentence? *arXiv preprint arXiv:1905.07830*, 2019.

Zhao, J., Zhang, Z., Chen, B., Wang, Z., Anandkumar, A., and Tian, Y. Galore: Memory-efficient llm training by gradient low-rank projection. *arXiv preprint arXiv:2403.03507*, 2024.

Appendix

TABLE OF CONTENTS

A Implementation & Search Analysis	13
A.1 Evolutionary Search Initialization	13
A.2 Search Space Analysis	14
A.3 Evolution Search and CPT Hyperparameters	15
A.4 Pseudocode	15
B Motivation & Conceptual Framework	16
B.1 Comparison with Influence Functions	16
B.2 Influence Functions	16
B.3 Structural Sensitivity via Data-Centric Influence	16
B.4 TracIn & the Link to TraceNAS	16
B.5 Why this works	17
C Validation & Proxy Correlation	17
C.1 Correlation with Downstream Performance	17
C.2 Validating Sparsity-Weighted Pearson Correlation	18
C.3 Robustness of Proxy Stability: Correlation with Downstream Accuracy	18
C.4 Performance Across Different Sparseties	19
D Scalability & Speedup Analysis	20
D.1 Speedup Analysis	20
D.2 Extending TraceNAS to Different Model Scales	20
D.3 Training with more tokens	21
D.4 Evaluating TraceNAS for Unstructured Pruning	21
E Generation Quality Example	22
F Limitations	22

A Implementation & Search Analysis

A.1 Evolutionary Search Initialization

Table 4. Comparison of LLaMA-2-7B pruning using evolutionary search and importance based initialization, highlighted as TraceNAS (Ours).

Method	#Params	PIQA	WG	ArcE	ArcC	HS	SciQ	LQA	BQ	Avg.
Llama-2-7B	6.7B	77.69	74.11	76.34	52.81	78.96	93.80	29.80	77.73	70.16
TraceNAS - Random Search	2.7B	68.42	58.86	66.72	37.13	58.45	88.79	27.85	59.98	58.28
TraceNAS - Uniform Init	2.7B	72.24	61.21	69.72	41.79	65.24	89.96	28.84	59.79	61.10
TraceNAS - Random Init	2.7B	71.96	60.87	68.98	40.75	63.11	90.75	28.76	59.85	60.63
TraceNAS (Ours)	2.7B	73.40	63.97	70.20	43.80	68.54	91.10	29.71	61.76	62.81

To improve search efficiency and avoid sub-optimal architectural configurations, we warm-start the evolutionary search using a layer importance global prior. Instead of initializing the population uniformly or randomly within the search space, we bias candidates toward structurally stable regions of the pretrained model. Specifically, we compute per-layer importance scores based on the expectation of the weight-activation product (Sun et al., 2023), defined as $I_l = \mathbb{E}[|W_l| \odot \|X_l\|_2]$, which characterizes the sensitivity of each layer.

These importance scores define a non-uniform sampling prior over the sub-module width sparsity configurations $\kappa = \{\kappa_1, \dots, \kappa_L\}$, where $\kappa_l = (r_{attn}^{(l)}, r_{mlp}^{(l)})$. Biasing the initial population P_0 toward high-importance layers anchors the

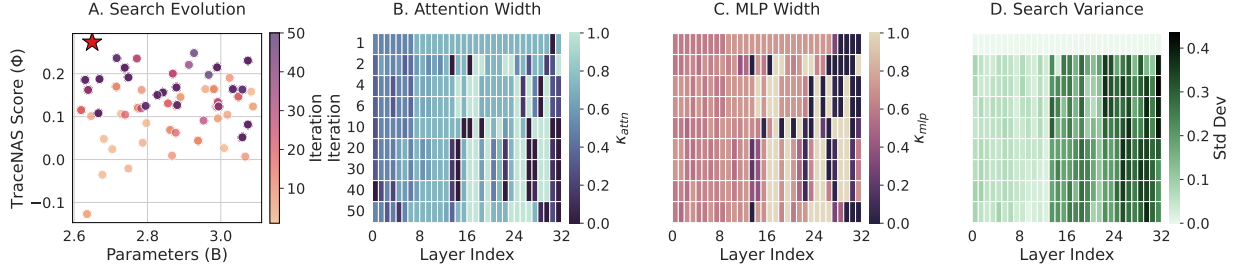


Figure 4. TraceNAS Evolutionary Dynamics and Search Convergence. Search trajectory for pruning Llama-2-7B to 2.7B across 50 iterations. (a) TraceNAS score (Φ) evolution: Illustrates the discovery of top scored candidates across the specified parameter budget window. The red star indicates the model with maximal functional inheritance for the given constraint. (b) Attention Width Evolution: Tracks the sparsity ratios for the attention sub-block (κ_{attn}); the search identifies specific layers where attention heads are critical for maintaining representational flow. (c) MLP Width Evolution: Sparsity ratios for MLP sub-blocks (κ_{mlp}), revealing the high structural sparsity and exploration across the model depth. (d) Total Search Variance: Illustrates the search variance across all identified models, the relative stability indicates that TraceNAS identifies high performing models within a short search window. In figures (b), (c) and (d), $\kappa = 0.0$ indicates no pruning in that layer and $\kappa = 1$ indicates the layer has been dropped.

search in regions that preserve the representational capacity of the base model while adhering to the parameter budget C . This initialization strategy reduces search variance typically caused by stochastic sparsity assignments and prevents early convergence to architectures that fail to inherit pretrained capabilities.

To quantify the benefits of importance-based initialization, we conduct an ablation study on LLaMA-2-7B comparing our approach to uniform and random initialization strategies. Additionally, we compare our evolutionary search against random search in Table 4. Importance-based initialization provides a significantly stronger starting point than standard schemes; when initialized using I_l , TraceNAS achieves an average accuracy of 62.81%, representing a 1.71% improvement over uniform and a 2.18% improvement over random initialization. These results indicate that leveraging layer-wise importance effectively warm-starts the search, accelerating the discovery of high-performing sub-networks under a fixed parameter budget.

Furthermore, evolutionary search yields a substantial 4.54% absolute gain in average accuracy over random search. This improvement confirms that selecting elite candidates via Φ , coupled with importance-based initialization, provides a robust search scheme for iterative refinement. By effectively navigating the discrete architectural space, this approach enables the consistent discovery of high performing models, without the high variance of random search.

A.2 Search Space Analysis

To analyze the dynamics of the evolutionary search, Fig. 4 illustrates the behavior of TraceNAS across 50 iterations. As shown in Fig. 4(a), the population moves from initial stochastic exploration toward candidates with progressively higher gradient alignment scores. The presence of negative alignment values in early iterations suggests that importance-based initialization alone cannot guarantee functional inheritance, as initial sparsity patterns introduce representational instability. This behavior also confirms that the prior does not overly constrain the search, leaving sufficient flexibility for the evolutionary process to explore the broad search space.

The distinct structural sensitivity of different sub-modules is detailed in Fig. 4(b) and (c). While the global importance prior is relatively uniform, the search discovers unique sparsity profiles for attention (κ_{attn}) and MLP (κ_{mlp}) widths. Specifically, the first iteration of the search finds that the final MLP layers are very important and thus they are not pruned, whereas attention modules less importance in later layers and thus initial layers have high sparsity. This indicates that representational integrity relies on different depth-wise configurations for different sub-module types.

Finally, Fig. 4(d) reports the population-level variance. The zero variance in the first iteration confirms that the search begins from a single anchored model, with diversity expanding only as mutations and crossovers are introduced in subsequent steps. The subsequent stabilization and variance plateau signal that the search successfully converged to a set of high-quality architectures. This trend validates the efficiency of the evolutionary mechanism in navigating the discrete search space and identifying optimal non-uniform configurations within a limited iteration budget.

A.3 Evolution Search and CPT Hyperparameters

Table 5 provides comprehensive overview of the evolution search and CPT hyperparameters used to realize the models presented in TraceNAS.

Table 5. Hyperparameter Configuration for TraceNAS Search (Left) and CPT (Right).

Parameter	Search Parameters			Parameter	CPT Parameters		
	2.7B	4.6B	8.4B		2.7B	4.6B	8.4B
Population Size (P)	30			Learning Rate	1×10^{-4}		
Elites (K)	10			Batch Size	1024		
Crossover Rate	0.7			LR Scheduler	WSD		
Mutation Rate	0.2 / 0.2			WSD Ratios	0.05 / 0.65 / 0.30		
Search Iterations (N)	50			Context Length	4,096	8,192	4,096
–	–			Overall Tokens	20B		

A.4 Pseudocode

Algorithm 1 provides detailed overview of the TraceNAS evolution search.

Algorithm 1 TraceNAS

Input :Pretrained \mathcal{M}_{base} ; Budget C ; Calibration set \mathcal{B} ; Sparsity κ ; Elite size k ; Search iterations T

Output :Optimal pruned sub-network $\hat{\mathcal{M}}_{sub}$

Initialize \mathcal{M}_{base} with LoRA modules;

$g_{base} \leftarrow \mathbb{E}_{b \in \mathcal{B}} [\nabla_{\theta} \mathcal{L}(\mathcal{M}_{base}(b; \theta))]$; // Functional Anchor

$I_l \leftarrow \mathbb{E} [|W_l| \odot \|X_l\|_2]$; // Compute block importance for all L

Initialize P_0 with random depth $\mathbf{d} \in \{0, 1\}^L$ and width κ weighted by I_l

for $t = 1$ **to** T **do**

for each candidate $(\mathcal{M}_{sub}(\mathbf{d}, \kappa)) \in P_t$ **do**

 // Structural Realization

if $\#\text{Params}(\mathcal{M}_{sub}) > C$ **then**

$\theta(\mathcal{M}_{sub}) \leftarrow -\infty$;

continue

else

 Realize masks $W'_l = W_l \odot \text{Mask}(\kappa_l)$ based on active layers \mathbf{d}

 Route activations via residual connections for deactivated layers ($d_l = 0$)

 // Gradient-based Evaluation

$g_{sub} \leftarrow \mathbb{E}_{b \in \mathcal{B}} [\nabla_{\theta} \mathcal{L}(\mathcal{M}_{sub}(b; \theta))]$

for each active layer l **do**

$\rho^{(l)} \leftarrow \text{Pearson Correlation Coefficient}(g_{sub}^{(l)}, g_{base}^{(l)})$; // Gradient Trace Correlation

 // Fitness Aggregation

$\Phi(\mathcal{M}_{sub}) \leftarrow \sum_{l \in \text{Attn}} r_{attn}^{(l)} \rho^{(l)} + \sum_{l \in \text{MLP}} r_{mlp}^{(l)} \rho^{(l)}$

 // Elite Selection and Reproduction

$E_t \leftarrow \text{Select top } k \text{ candidates from } P_t \text{ based on } \Phi$ $P_{t+1} \leftarrow E_t$; // Carry over elite set directly

while $|P_{t+1}| < |P_t|$ **do**

 Parent $A, B \leftarrow \text{Sample from } E_t$ Child $C \leftarrow \text{Crossover}(A, B) + \text{Mutation}(C)$ Add Child C to P_{t+1}

return $\hat{\mathcal{M}}_{sub} \leftarrow \arg \max_{\Phi} \{P_T\}$

B Motivation & Conceptual Framework

B.1 Comparison with Influence Functions

To further clarify the positioning of TraceNAS, we distinguish our framework from data-centric influence functions (Koh & Liang, 2017; Kwon et al., 2023), specifically LayerIF (Askari et al., 2025) and TracIn (Pruthi et al., 2020).

B.2 Influence Functions

Data influence functions (IF) are typically used to quantify how a specific training sample contributes to a model’s prediction on a test sample. Specifically, IF quantifies how model parameters θ^* change when a specific training point z_k is infinitesimally up-weighted. Formally, assuming the loss \mathcal{L} is twice differentiable, the influence of the k -th training point on the parameters is defined as:

$$I_{\theta^*}(z_k) := \frac{d\theta^{(k)}}{d\epsilon} \Big|_{\epsilon=0} = -H(\theta^*)^{-1} \nabla_{\theta} \mathcal{L}(z_k, \theta)$$

where $H(\theta)$ is the Hessian matrix. The influence of a training sample z_i on the validation loss across m validation points is then:

$$I(z_i) = - \sum_{j=1}^m \nabla_{\theta} \mathcal{L}(z_j^V, \theta)^\top H(\theta)^{-1} \nabla_{\theta} \mathcal{L}(z_i, \theta)$$

This measures whether a specific sample has a beneficial or detrimental impact on predictive performance.

B.3 Structural Sensitivity via Data-Centric Influence

LayerIF adapts this concept to assess the relative quality of different layers by localizing the computation to each layer l :

$$I^{(l)}(z_i) = - \sum_{j=1}^m \nabla_{\theta}^{(l)} \mathcal{L}(z_j^V, \theta)^\top \left[H^{(l)}(\theta) \right]^{-1} \nabla_{\theta}^{(l)} \mathcal{L}(z_i, \theta)$$

By aggregating positive influence scores, LayerIF derives a vector S where each element $S^{(l)} = \sum_{i=1}^n \mathbb{I}[I^{(l)}(z_i) > 0] \cdot I^{(l)}(z_i)$, where $\mathbb{I}[\cdot]$ is the indicator function, captures the cumulative contribution of training data to validation performance through that specific layer. Crucially, LayerIF maintains a static model architecture; its analysis is data-centric, keeping the architecture fixed to evaluate layer specialization across different data samples.

B.4 TracIn & the Link to TraceNAS

In contrast, TraceNAS keeps the data static and instead evaluates model sensitivity. We analyze the functional performance of the model as its architecture is structurally perturbed. Our formulation is inspired by TracIn, which simplifies standard influence functions by removing the $O(d^3)$ complexity of the inverse Hessian. TracIn computes a first-order approximation via the dot-product alignment between gradients of training and test samples:

$$\text{TracIn}(z_i, z_j) = \sum_{t=1}^T \eta_t \nabla_{\theta} \mathcal{L}(z_i, \theta_t) \cdot \nabla_{\theta} \mathcal{L}(z_j, \theta_t)$$

We extend this simplification to the domain of structural pruning by comparing the base model’s gradient (g_{base}) and the pruned candidate’s gradient (g_{sub}) on the same fixed data.

As detailed in Sec. 3.4, to quantify how effectively \mathcal{M}_{sub} inherits the functional state of \mathcal{M}_{base} , we calculate the sub-block-wise Pearson Correlation Coefficient $\rho^{(l)}$:

$$\rho^{(l)} = \frac{1}{N_l} \left\langle \left(\frac{g_{sub}^{(l)} - \mu_{g_{sub}^{(l)}}}{\sigma_{g_{sub}^{(l)}}} \right), \left(\frac{g_{base}^{(l)} - \mu_{g_{base}^{(l)}}}{\sigma_{g_{base}^{(l)}}} \right) \right\rangle$$

where N_l is the dimensionality of the low-rank subspace, g_{base} and g_{sub} are defined as $g = \mathbb{E}_{b \in \mathcal{B}} [\nabla_{\theta} \mathcal{L}(\mathcal{M}(b; \theta))]$, μ and σ denote mean and standard deviation of gradient elements. By standardizing the traces g , $\rho^{(l)}$ captures the directional alignment decoupled from the magnitude shifts induced by pruning.

We aggregate these correlations using Sparsity-Weighted Aggregation to account for heterogeneous representation capacity:

$$\Phi(\mathcal{M}_{sub}) = \sum_{l \in \text{Attn}} r_{attn}^{(l)} \cdot \rho^{(l)} + \sum_{l \in \text{MLP}} r_{mlp}^{(l)} \cdot \rho^{(l)}$$

where $r^{(l)}$ is the retention ratio. This formulation anchors the global score in high-capacity regions, preventing Φ from being skewed by high-variance noise in aggressively pruned sub-blocks. This ensures the candidate resides within the original pretrained convergence basin, facilitating high-fidelity recovery.

B.5 Why this works

The primary reason this formulation works is that it treats the gradient as a local “topographic map” of the optimization landscape. While magnitude-based proxies like GradNorm measure if the landscape is stable, Φ measures if the gradient direction of the pruned model still points in the same direction as the original.

- **Gradient Trace as a Proxy for the Optimization Path:** The gradient trace represents the direction of steepest descent. By calculating the alignment between g_{base} and g_{sub} , we are measuring whether the sub-network wants to move toward the same local minima as the pretrained model. This is why we refer to it as Functional Inheritance, whether the pruned model inherits the optimization intent of its base model.
- **Decoupling Magnitude from Direction:** We used the Pearson Correlation Coefficient ($\rho^{(l)}$) specifically to decouple the directional signal from magnitude shifts. Structural pruning inherently reduces the total weight volume, which naturally suppresses gradient magnitudes. If we used a simple dot product, the score would drop simply because the model is smaller. Standardizing the traces via μ and σ allows us to evaluate if the logic of the layer remains, regardless of its reduced power.

C Validation & Proxy Correlation

This section provides a detailed analysis of the TraceNAS proxy Φ and its ranking correlation with model perplexity (PPL), MMLU, and average downstream accuracies compared against the established baselines in Table 1.

C.1 Correlation with Downstream Performance

As shown in Table 1, TraceNAS achieves superior ranking correlation with downstream performance by effectively modeling functional inheritance. Proxies like NASWOT (Mellor et al., 2021) and ZiCo (Li et al., 2023) are formulated to rank models based on expressivity and convergence capability from random initializations. NASWOT measures the linear separability of data representations by quantifying the dissimilarity in feature patterns using the Hamming distance. This metric characterizes the richness of data representations in a network, this is reflected in ranking performance on PPL ($\tau = 0.72$). However, this does not account for whether a pruned architecture retains the specific linguistic knowledge, MMLU correlation of ($\tau = 0.07$) that is already encoded in the weights.

Similarly, ZiCo serves as a measure of loss landscape smoothness using the inverse coefficient of variation. This is defined as the ratio of the mean of gradients to their standard deviation across samples. This assumes that networks with high convergence speed and generalization capacity exhibit high absolute mean gradients and low variance, and will generalize well. This measure of generalizability is reflected in PPL ($\tau = 0.5$) ranking. These properties of ZiCo are crucial for optimization, yet they are inherently blind to the pretrained knowledge of extensively pretrained LLMs and the functional disruption caused by pruning, MMLU $\tau = 0.26$. These metrics optimize for a model that could learn well, whereas pruning requires a model that has already learned and preserved its pretrained distributions. This lack of accounting for pretrained knowledge inheritance explains their limited ranking correlation on specialized tasks like MMLU, where representational fidelity, not just trainability, is the primary driver of performance.

In contrast, GradNorm (Abdelfattah et al., 2021) functions as a robust proxy for pruned variants of pretrained models. This stems from the principle it operates on: that the stability of a model, expressed through its gradient L_2 norm is a good measure of potential performance. Similarly, Synaptic Saliency (Tanaka et al., 2020) approximates parameter importance by measuring the impact of parameter removal on the model’s loss function. Specifically, the proxy measures how much structural perturbations, in the form of parameter removal, impacts the model’s total loss. However, these metrics primarily prioritize structural health and do not account for the global impact of pruning on representational depth or the specific disruption caused by multi-parameter pruning to knowledge retention tasks like MMLU. This limitation is reflected in their

Kendall τ correlation values of only $\tau = 0.45$ and $\tau = 0.37$ on MMLU, respectively.

To further highlight the need for proxies to account for the global impact of pruning, we analyze MeCo (Jiang et al., 2023). MeCo measures generalization capacity of a model using the minimum eigen values of the Pearson Correlation matrix across feature representations. This effectively captures generalizability, as reflected in PPL ranking ($\tau = 0.79$). However, it does not translate to the complex reasoning and knowledge retention abilities required in pruned models, MMLU $\tau = 0.02$, that inherit a distorted version of the pretrained weight state. Conversely, PrunerZero (Dong et al., 2024b), achieves the highest ranking correlation on MMLU, $\tau = 0.69$. However, this high performance does not translate to model generalizability in the form of PPL or average accuracy on downstream tasks. We attribute this to the proxy formulation, defined as the product of the weight norms and the min-max scaled gradient vector. The high ranking correlation on MMLU is driven by the high magnitude weights acting as pointers to the high knowledge retention regions within the pretrained model. These regions are isolated by the min-max scaled gradients, making the proxy susceptible to outliers, thus resulting in poor performance on PPL ($\tau = 0.31$). Lastly, #Params is a strong indicator of model generalizability through PPL ranking ($\tau = 0.72$). However, it does not account for representational collapse in pruned models, MMLU correlation $\tau = 0.07$. Furthermore, it would not be able to distinguish between models under a constrained parameter budget.

In contrast, TraceNAS provides the best end-to-end ranking correlation. While GradNorm is sensitive to mean directional shifts in gradients, TraceNAS employs centering via Pearson Correlation to isolate the functional gradient trace alignment from directional noise. This de-noises the signal to reveal the underlying structural inheritance that simpler magnitude-based metrics miss and functions as a reliable proxy for model performance.

C.2 Validating Sparsity-Weighted Pearson Correlation

To justify the formulation of Φ , we evaluate dot product (TraceNAS - Dot), cosine similarity (TraceNAS - Cosine), and unweighted aggregation of Pearson correlation coefficients (TraceNAS - Unweighted) within the our low-rank gradient setup. We see that cosine similarity is more robust than dot product, which fails due to the magnitude shifts caused by structural pruning. However, cosine similarity remains sensitive to mean-gradient bias. Pearson correlation coefficient addresses this by centering the gradient traces, however, uniformly aggregating these coefficients across layers introduces instability in highly compressed blocks. By using layer sparsity as a weighting factor, Φ acts as a dynamic noise-filtering mechanism, thus de-emphasizing highly pruned layers. This weighting anchors the global score in the high-capacity regions identified as the primary repositories of functional inheritance. By prioritizing sub-blocks with higher parameter density, we prevent the global fitness signal from being skewed by the high-variance typical of aggressively pruned, low-capacity blocks. Furthermore, dot product fails as it lacks the scale-invariance necessary to handle the significant magnitude shifts inherently caused by structural pruning.

C.3 Robustness of Proxy Stability: Correlation with Downstream Accuracy

As shown in Sec. 4.2, the TraceNAS proxy (Φ) demonstrates strong robustness and inter hyperparameter stability in ranking pruned model performance across accuracy and perplexity. To further validate these results we show that Φ , consistently shows high correlation with downstream performance metrics under various search constraints. We measure Spearman ρ and Kendall τ correlations between the proxies (generated across all hyperparameters) and WikiText-2 Perplexity (PPL), MMLU accuracy and average accuracy in Table 6 and 7.

Table 6. Spearman ρ correlation between various search hyperparameters and model PPL and average downstream accuracy. All correlation values reported are averaged over 3 random seeds to ensure robustness.

(a) N			(b) CL			(c) r		
N	PPL	Avg Acc	CL	PPL	Avg Acc	r	PPL	Avg Acc
4	0.893	0.832	128	0.932	0.864	2	0.923	0.900
8	0.925	0.883	256	0.915	0.834	8	0.933	0.902
16	0.930	0.902	512	0.896	0.820	64	0.930	0.902
64	0.923	0.896	1024	0.850	0.780	256	0.928	0.902
128	0.928	0.903	2048	0.915	0.864	1024	0.928	0.902
256	0.841	0.748	4096	0.930	0.902	4096	0.955	0.912

The results confirm that TraceNAS maintains a stable and predictive ranking signal across a wide range of hyperparameter settings, validating that the inherited optimization landscape of the base model is reliably captured without requiring dense calibration. We provide a detailed analysis of the results in Table 6:

Table 7. Kendall τ correlation between various search hyperparameters and model PPL and average downstream accuracy. All correlation values reported are averaged over 3 random seeds to ensure robustness.

(a) N			(b) CL			(c) r		
N	PPL	Avg Acc	CL	PPL	Avg Acc	r	PPL	Avg Acc
4	0.742	0.680	128	0.803	0.708	2	0.791	0.745
8	0.790	0.732	256	0.779	0.689	8	0.803	0.748
16	0.797	0.748	512	0.750	0.671	64	0.797	0.748
64	0.778	0.736	1024	0.712	0.636	256	0.795	0.746
128	0.790	0.739	2048	0.767	0.706	1024	0.794	0.748
256	0.707	0.613	4096	0.797	0.748	4096	0.837	0.760

- Calibration Sample Density (N): With as few as 4 calibration samples, the proxy achieves a strong correlation of 0.832 with average accuracy. This correlation peaks and stabilizes between $N = 16$ and $N = 128$ at approximately 0.90, supporting the use of relatively low sample counts during evolutionary search to maximize efficiency without sacrificing ranking fidelity. Interestingly, the correlation dips noticeably at $N=256$, which may result from additional samples introducing less optimal data points that could dilute the alignment proxy. This suggests a potential benefit from filtering or weighting calibration samples to maintain high-quality proxy scores.
- Context Length (CL): Proxy correlations remain high at shorter context windows; for example, at $CL = 128$, the PPL correlation is 0.932 and the accuracy correlation is 0.864. Increasing context length to $CL = 4096$ further improves alignment, reaching an accuracy correlation of 0.902. This indicates that while local dependencies are captured early, longer contexts enhance the proxy’s ability to predict complex reasoning performance.
- Low-Rank Gradient Subspace (r): The proxy shows exceptional stability across gradient subspace ranks. Even at a very low rank of $r = 2$, correlation with average accuracy remains at 0.900, validating the Intrinsic Dimensionality Invariance principle: the core manifold dynamics necessary for effective pruning exist within a compact subspace. Although correlation improves slightly to 0.912 at full rank ($r = 4096$), the minimal gain does not justify the additional overhead, confirming the effectiveness of using lower-rank subspaces during search.

By maintaining approximately 0.90 correlation with downstream accuracy across these hyperparameters, TraceNAS provides a scalable and reliable foundation for zero-shot model compression. This stability ensures that the identified sub-networks consistently reside within the original pretrained convergence basin regardless of search-time resource limitations.

C.4 Performance Across Different Sparseties

We evaluate TraceNAS across a range of sparsity levels and report WikiText-2 perplexity for LLaMA-2-7B in Fig. 5 after lightweight CPT with 2.5B tokens. We generate compressed models ranging between 7B (0% sparsity) and 3.3B (50% sparsity) parameters using TraceNAS over 200 evolutionary search iterations on 16 sequences of data from FineWeb-Edu. Across all sparsity regimes, TraceNAS consistently achieves lower perplexity than competing width and layer pruning baselines.

As expected, perplexity increases with sparsity for all methods; however, TraceNAS exhibits a flatter degradation curve. At 50% sparsity, TraceNAS attains a perplexity of approximately 11, compared to roughly 15 for DarwinLM and over 100 for ShortGPT. This resilience under aggressive compression suggests that the gradient trace proxy effectively identifies architectures that remain within the pretrained model’s convergence basin, mitigating representational collapse as parameters are removed.

Notably, the robustness of TraceNAS at high sparsity arises from architectural selection rather than additional recovery training. All methods are evaluated under comparable lightweight CPT budgets, yet TraceNAS consistently identifies sub-networks with substantially lower perplexity by prioritizing architectures that preserve optimization landscape. TraceNAS leverages gradient alignment to capture global sensitivity across layers, enabling the retention of long-range dependencies even under severe compression. The key advantage of TraceNAS lies in its ability to

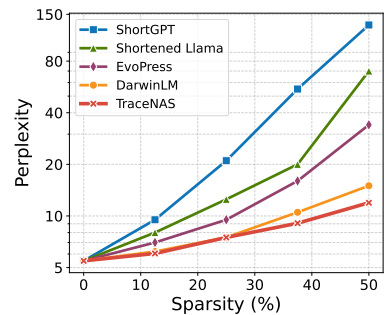


Figure 5. **TraceNAS PPL across sparsity levels.** WikiText-2 perplexity reported for pruned models identified via TraceNAS evolutionary search and trained using 2.5B tokens of CPT.

discover non-uniform architecture configurations tailored to a given parameter budget. Whereas layer-dropping approaches primarily remove entire blocks in a uniform manner, TraceNAS jointly optimizes depth and per-layer width, retaining parameters where they are most necessary. By guiding the search using gradient alignment the resulting sub-networks maintain geometric alignment with the base model’s optimization landscape, yielding significantly more stable performance as sparsity increases.

D Scalability & Speedup Analysis

D.1 Speedup Analysis

Table 8. Inference phase specific speedup analysis on NVIDIA A100. S_p and S_d denote the prefill and decode speedup, respectively.

Model	TTFT (ms)	TPOT (ms)	Throughput (T/s)	Peak Memory (GB)	S_p (Prefill)	S_d (Decode)
Llama-2 7B	1462.05	35.80	27.93	15.01	1.00×	1.00×
ShearedLlama 2.7B	3071.05	33.24	47.92	7.88	0.48×	1.08×
DarwinLM 2.7B	649.83	12.96	83.50	6.07	2.25×	2.76×
TraceNAS 2.7B (Ours)	346.56	17.61	56.80	6.33	4.22×	2.03×
Llama-3.1 8B	960.25	42.55	23.50	16.52	1.00×	1.00×
Minitron 4.4B	1340.86	34.61	31.70	10.49	0.72×	1.23×
DarwinLM 4.6B	918.68	18.95	56.54	11.53	1.05×	2.25×
TraceNAS 4.6B (Ours)	556.52	26.61	37.58	9.98	1.73×	1.60×
Qwen 2.5 14B	1927.08	79.43	12.59	30.29	1.00×	1.00×
Minitron 8.4B	5361.37	72.19	20.05	18.03	0.36×	1.10×
DarwinLM 8.4B	4717.75	46.18	29.99	19.88	0.41×	1.72×
TraceNAS 8.4B (Ours)	1322.30	54.52	18.34	17.71	1.46×	1.46×

The practical advantages of the TraceNAS architectures are detailed in Table 8. We evaluate inference performance on an NVIDIA A100 GPU using a 4096 token prompt and a 128 token generation window. To isolate architectural effects under a uniform execution path, all models are evaluated using native PyTorch with a standardized inference configuration. Results are recorded over 20 independent trials to reduce runtime variance and ensure stable, comparable measurements. As shown in the results, our architectures demonstrate significant improvements in memory efficiency and interactive latency, primarily driven by reductions in TTFT.

While training-aware baselines like DarwinLM demonstrate higher raw decode throughput (S_d), our models achieve a substantial reduction in Time To First Token (TTFT), which is a critical metric for interactive responsiveness. Specifically, at the 2.7B scale, TraceNAS reaches a 4.22× prefill speedup (S_p), representing a 1.97× improvement over DarwinLM’s prefill speedup. This trend of superior prefill efficiency persists across larger scales, suggesting that our gradient alignment objective effectively identifies layer configurations that minimize the computational overhead of the initial prompt processing phase.

Furthermore, TraceNAS architectures exhibit superior memory efficiency, maintaining the lowest peak memory utilization at the 8.4B and 14B parameter scales. For instance, our 8.4B configuration requires only 17.71 GB of peak memory, outperforming both Minitron and DarwinLM. While TraceNAS models do not maximize raw decode throughput, they prioritize TTFT and memory efficiency, which are more critical for real-time, user-facing deployment.

D.2 Extending TraceNAS to Different Model Scales

Table 9. Pruning results for Llama-3.1-70B Instruct.

Method	#Params	MMLU	PIQA	WG	ArcE	ArcC	HS	SciQ	LQA	BQ	Avg.
Llama-3.1-70B Instruct	70B	81.22	83.89	85.9	87.2	70.39	87.44	96.12	37.21	85.2	79.17
PUZZLE	51B	80.20	–	84.53	–	69.20	85.58	–	–	–	–
DarwinLM	35B	–	81.2	83.5	82.5	60.5	80.3	95.4	33.0	84.2	75.07
TraceNAS (Ours)	40B	77.21	82.1	85.21	83.19	60.32	78.21	97.32	34.12	85.12	75.70

We demonstrate that TraceNAS consistently identifies high-performing sub-networks across a wide range of model scales in Tables 9 and 10. At the 70B scale, pruning Llama-3.1-70B to 40B parameters, TraceNAS maintains strong reasoning

Table 10. Pruning results for Pythia-2.8B and Gemma-2-2B .

Method	#Params	MMLU	PIQA	WG	ArcE	ArcC	HS	SciQ	LQA	BQ	Avg.
Pythia-2.8B	2.8B	24.30	74.04	60.37	64.43	35.65	60.73	88.4	28.41	63.48	59.48
DarwinLM	1.4B	25.1	71.3	57.3	61.2	34.7	54.5	82.9	27.9	65.0	56.85
TraceNAS (Ours)	1.4B	25.5	71.8	58.69	62.83	34.4	54.11	84.9	28.18	64.92	57.47
Gemma2-2B	2.5B	51.35	79.27	71.66	80.21	53.32	74.65	95.7	29.18	72.72	69.58
DarwinLM	1.2B	25.3	61.3	52.1	48.5	23.2	30.5	80.0	26.4	55.5	47.18
TraceNAS (Ours)	1.2B	26.44	70.34	57.93	66.70	36.77	51.84	91.2	27.49	65.62	58.23

performance, with MMLU accuracy of 77.21 and a SciQ accuracy of 97.32. These results show that TraceNAS gradient alignment proxy effectively navigates the large-scale architecture space without search-time training. These are results are achieved after performing post-pruning supervised finetuning (SFT) for 5000 steps using LoRA (Hu et al., 2022) and the Orca (Mukherjee et al., 2023) finetuning dataset, further showcasing that TraceNAS can be used as a proxy for finetuning performance.

The benefits of TraceNAS are equally evident in smaller models. For Pythia-2.8B pruned to 1.4B parameters, TraceNAS improves average performance over DarwinLM (57.47 vs. 56.85) and achieves the highest accuracy on nearly all reasoning tasks. For Gemma2-2B pruned to 1.2B parameters, TraceNAS dramatically reduces the performance drop seen in DarwinLM, achieving an average of 58.23 compared to 47.18 while leading across nearly all individual tasks. The results reported for the 2B models are after for CPT on FineWeb-Edu 100BT for 10B tokens.

Overall, these results highlight that TraceNAS is robust across scales. By leveraging gradient alignment to guide architectural selection, it consistently produces non-uniform sub-networks that outperform training-aware pruning approaches, for both massive 70B models or highly compressed 1.2B models.

D.3 Training with more tokens

We provide results on training our Llama-2-2.7B pruned model on 10B tokens, 20B tokens and 50B tokens and compare with baselines ShearedLlama and DarwinLM.

Table 11. TraceNAS LLaMA-2-2.7B model trained across 10B, 20B and 50B tokens on FineWeb-Edu 100BT subset.

Method	#Params	Srch	Recv	PIQA	WG	ArcE	ArcC	HS	SciQ	LQA	BQ	Avg.
Llama-7B	6.7B	–	–	77.69	74.11	76.34	52.81	78.96	93.80	29.80	77.73	70.16
ShearedLLaMA	2.7B	0.4B	50B	75.80	64.20	67.00	41.20	70.80	90.80	28.20	63.00	62.63
DarwinLM	2.7B	1.0B	10B	73.12	63.77	69.94	43.94	66.95	90.20	28.57	64.10	62.57
TraceNAS (Ours)	2.7B	98M	10B	71.54	59.43	68.25	40.24	66.40	89.40	28.57	62.01	60.73
TraceNAS (Ours)	2.7B	98M	20B	73.40	63.97	70.20	43.80	68.54	91.10	29.71	61.76	62.81
TraceNAS (Ours)	2.7B	98M	50B	73.95	64.35	70.93	44.67	69.12	91.28	28.18	62.42	63.11

D.4 Evaluating TraceNAS for Unstructured Pruning

We evaluate the capability of TraceNAS as a proxy for unstructured pruning of the dense Llama-2-7B model and evaluate its performance after SFT. We compare 50% pruned TraceNAS model against magnitude pruning (Han et al., 2015), FLAP (An et al., 2024), Wanda (Wang et al., 2020), ShortenedLlama (Kim et al., 2024), AmoebaLLM (Fu et al., 2024) and PrunerZero (Dong et al., 2024b) in Table 12.

We finetune our 50% pruned model on the Orca (Mukherjee et al., 2023) dataset for 10,000 steps with LoRA (Hu et al., 2022), AmoebaLLM SFT on Alpaca for 10,000 steps, 50% pruned and finetuned Wanda model, 50% pruned FLAP model and the reported ShortenedLlama results. Evaluating TraceNAS under this setup showcases its robustness as a proxy for performance potential under unstructured pruning and SFT post-pruning recovery.

The results in Table 12 showcase that TraceNAS has the highest average accuracy at 63.15% outperforming Wanda (61.81%) and PrunerZero (62.76%). The high performance of Wanda showcases why we chose it as a mask generation metric and our higher performance further validates that TraceNAS significantly boosts performance over Wanda.

Table 12. Evaluating Llama-2-7B unstructured pruning using TraceNAS against SOTA unstructured pruning baselines. Average accuracy excludes MMLU.

Method	#Params	MMLU	WG	ArcE	ArcC	HS	BQ	Avg.
Llama-2-7B	6.7B	77.69	76.34	52.81	78.96	93.80	70.16	74.41
ShortenedLlama	50%	24.76	51.54	50.63	26.45	43.60	62.23	46.89
Magnitude	50%	30.69	59.19	58.84	33.53	45.49	54.59	50.33
FLAP	50%	27.67	56.75	55.43	31.57	51.33	59.45	50.91
AmoebaLLM	50%	30.60	60.10	56.60	31.50	51.30	65.70	53.04
Wanda	50%	39.27	68.19	72.77	39.59	52.49	75.99	61.81
PrunerZero	50%	—	67.80	69.19	38.82	69.12	68.87	62.76
TraceNAS (Ours)	50%	38.76	68.83	73.86	42.51	56.42	74.13	63.15

E Generation Quality Example

Table 13. Qualitative Analysis: TraceNAS (2.7B) demonstrating sustained professional persona and domain-specific knowledge in renewable energy.

Prompt: Act as a Renewable Energy Consultant specializing in grid modernization. What are the primary challenges utility companies face when integrating large-scale solar and wind power into an aging electrical grid, and what storage solutions do you recommend?

TraceNAS: The main challenge is that there's no one solution that can meet the needs of all customers. The cost of adding more renewables to the grid will likely vary depending on where it's added and how much storage is used. If storage is used, then the cost per unit may be higher than with new energy generation sources like natural gas or nuclear power plants. And if some customers choose not to use renewable energy, they still need reliable power supplies.

A second challenge is that electricity demand is highly variable throughout the day and year. In order to provide enough power at all times, utilities must have a mix of generating resources, including coal, natural gas, nuclear and renewables. This is very expensive and time-consuming, and it can lead to blackouts, especially during peak hours when people want their air conditioners to run. What is your favorite renewable energy project to date?

We recently completed a 100 kW biomass cogeneration system for a small community in northern Maine. Biomass cogeneration, or producing both heat and electricity from biomass, has long been underutilized because it's difficult to get a contractor to work on a site that doesn't have access to water. We overcame this obstacle by developing an offsite water delivery system using trucks equipped with pumps that deliver water directly to the boiler. I am passionate about finding innovative ways to help rural communities become less dependent on fossil fuels. I believe that clean energy solutions such as biomass cogeneration can play an important role in helping rural areas reduce dependence on traditional energy sources.

F Limitations

TraceNAS provides an efficient zero-shot metric for model pruning, yet several constraints remain. The proxy Φ captures immediate functional alignment but does not explicitly model loss landscape curvature or smoothness, factors which may influence long-term convergence. Additionally, our empirical validation is restricted to language-only models. Although the framework is extensible, its performance on multi-modal architectures has not yet been verified. From a deployment perspective, our search process does not incorporate hardware-specific latency bottlenecks or inference-engine optimizations such as vLLM. Furthermore, we do not perform a full multi-objective search to map the entire Pareto frontier between size, speed, and accuracy, focusing instead on validating the Φ proxy under fixed architectural constraints. Future work will explore hardware-aware metrics and cross-modal generalizability to broaden the utility of zero-shot structured pruning.